

# Channel Dynamics and SNR Tracking in Millimeter Wave Cellular Systems

Marco Giordani<sup>†</sup>, Marco Mezzavilla<sup>◇</sup>, Aditya Dhananjay<sup>\*◇</sup>, Sundeep Rangan<sup>◇</sup>, Michele Zorzi<sup>†</sup>

<sup>†</sup> University of Padova, Italy    <sup>◇</sup>NYU Wireless, Brooklyn, NY, USA    <sup>\*</sup>MilliLabs Inc., NY, USA  
emails: {giordani, zorzi}@dei.unipd.it, {mezzavilla, srangan}@nyu.edu, aditya@courant.nyu.edu

**Abstract**—The millimeter wave (mmWave) frequencies are likely to play a significant role in fifth-generation (5G) cellular systems. A key challenge in developing systems in these bands is the potential for rapid channel dynamics: since mmWave signals are blocked by many materials, small changes in the position or orientation of the handset relative to objects in the environment can cause large swings in the channel quality. This paper addresses the issue of tracking the signal to noise ratio (SNR), which is an essential procedure for rate prediction, handover and radio link failure detection. A simple method for estimating the SNR from periodic synchronization signals is considered. The method is then evaluated using real experiments in common blockage scenarios combined with outdoor statistical models.

**Index Terms**—Millimeter wave communication; cellular systems; radio frequency channel dynamics; filtering.

## I. INTRODUCTION

Each generation of wireless mobile technology has been driven by the need to meet new requirements that could not be completely achieved by its predecessor. Following this trend, fifth generation cellular (5G) systems are now expected to meet unprecedented speeds, near-wireline latencies and ubiquitous connectivity with uniform user Quality of Experience (QoE) [1], [2]. While current microwave bands below 3 GHz have become nearly fully occupied, the millimeter wave (mmWave) frequencies, roughly above 10 GHz, have enormous amounts of unused available spectrum. These bands are widely expected to become a key means of addressing the challenge of higher required data rates [3]–[5].

However, one of the key challenges for cellular systems in the mmWave bands is the rapid channel dynamics. In addition to the high Doppler shift, mmWave signals are completely blocked by many common building materials such as brick and mortar [6], and even the human body can cause up to 35 dB of attenuation [7]. As a result, the movement of obstacles and reflectors, or even changes in the orientation of a handset relative to a body or a hand, can cause the channel to rapidly appear or disappear.

This high level of channel variability has widespread implications for virtually every aspect of cellular design. This paper focuses on one particular important design issue which is the tracking of the downlink channel quality and signal-to-noise ratio (SNR) at the mobile user equipment (UE). Measuring the SNR and reporting the value in periodic *channel quality indicator* (CQI) reports is an essential component of any modern cellular system – see, for example [8], [9] for

a detailed description of the methods in 3GPP LTE. Most importantly, CQI reports are the basis for rate prediction and adaptive modulation and coding. While CQI errors can be mitigated somewhat via Hybrid ARQ (HARQ), HARQ requires retransmissions that may result in excess delay. One of the goals of 5G systems is to achieve very low ( $< 1$  ms) air link latencies. CQI and related signals measurements are also necessary for proper handover determination and radio link failure detection, which are likely to become more common in mmWave due to the small cell topology and the intermittency of the channel.

While CQI estimation is relatively straightforward in current cellular systems, there are at least three potentially complicating issues for mmWave: (i) the rapid dynamics due to blockage events that strongly affect the link quality; (ii) the need to track the CQI in multiple spatial directions with very narrow beams; and (iii) the limited number of available measurements since the *cell reference signal* (CRS) used in current 3GPP LTE systems may not be available for mmWave (see Section II-A).

To address these challenges, this paper presents two key contributions. First, we propose a novel method for estimating the channel quality using synchronization signals and directional scanning. This signaling mechanism was also considered for initial access in [10], [11]. We derive an unbiased estimate for the instantaneous wideband SNR in a particular pointing direction. The estimate can then be filtered over time to trade off noise reduction and tracking speed.

Secondly, we evaluate the SNR tracking through real measurements using a novel high-speed measurement system. There are currently a large number of measurements of mmWave outdoor channels and detailed statistical models [12]–[15]. However, these measurements have been largely performed in static locations with minimal local blockage. The dynamics of the channel are not fully understood – see some initial work in [16], [17]. In this work, we experimentally measure the dynamics of the channel in various common blockage scenarios using a high-speed channel sounder at 60 GHz. We then combine the measured channel traces with the statistical models to evaluate the SNR tracking algorithms.

## II. SYSTEM MODEL

### A. CQI Estimation in 3GPP LTE

CQI estimation of the downlink channel is relatively straightforward in 3GPP LTE [8], [9]: the downlink channel quality is measured from what is called the cell reference

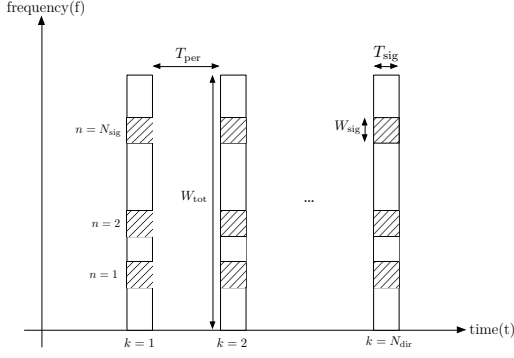


Figure 1: Periodic transmission of narrowband synchronization signals from the BS. This structure is similar to the LTE PSS.

signal (CRS). This is a wideband signal transmitted essentially continuously with one signal being sent from each BS cell transmit antenna port. Each UE in connected mode monitors these signals to create a wideband channel estimate that can be used both for demodulating downlink transmissions and for estimating the channel quality.

However, in addition to the rapid variations of the channel, there are two issues for CQI estimation in mmWave. First, a CRS will likely not be available since downlink transmissions at mmWave frequencies will be directional and specific to the UE. Demodulation reference signals will thus likely follow the format of LTE's UE-specific reference signals, which are transmitted in-band with the data. Thus, there will likely be no reference signals that are broadcast to all UEs. Secondly, mmWave UEs are likely to use analog beamforming, meaning that the UE can only measure the channel quality in one direction at a time [18], [19].

### B. Synchronization Signal Transmission Format

In the absence of CRS, each UE must find an alternate signal to measure the downlink channel quality. For this work, we propose that the UE estimates the channel quality from periodic synchronization signals similar to the LTE primary or secondary synchronization signals (PSS or SSS) used for initial access and cell search. These signals are transmitted at a much lower duty cycle and the estimation of the channel from these limited measurements is one of the key challenges addressed in this paper.

For the structure of the synchronization signals, we assume the format described in [10] and reported in Figure 1. Similar to the LTE PSS, we assume that each BS cell transmits a synchronization signal once every  $T_{\text{per}}$  seconds for a duration of  $T_{\text{sig}}$  seconds. These signals will be transmitted omnidirectionally or in a fixed pattern covering the cell area. Each transmission consists of  $N_{\text{sig}}$  sub-signals where each sub-signal is transmitted over a narrow band of  $W_{\text{sig}}$  Hz. The use of multiple transmissions is for frequency diversity.

At the UE side, we assume that the UE receiver attempts to estimate the received SNR of the synchronization signals in  $N_{\text{dir}}$  different angular directions. As discussed above, we

assume the UE performs analog beamforming and hence can measure the synchronization signal in only one direction at a time. We thus assume that in each synchronization signal period, the UE measures the received signal strength in one of the  $N_{\text{dir}}$  angular directions. Hence, it can make a received signal measurement in a particular angular direction once every  $N_{\text{dir}}T_{\text{per}}$  seconds. The specific parameter values will be discussed in Section IV.

### C. Channel Model and SNR Tracking

Let  $p_{ik}(t)$  be the  $k$ -th transmitted sub-signal in the  $i$ -th synchronization period. Let  $t_i$  denote the time of the synchronization period and  $f_k$  the frequency location of the sub-signal within that period. We assume that the sub-signal is received at the receiver as

$$r_{ik}(t) = \mathbf{w}_i^{rx*} \mathbf{H}(t_i, f_k) \mathbf{w}_i^{tx} p_{ik}(t) + n_{ik}(t),$$

where  $\mathbf{w}_i^{rx}$  is the RX beamforming vector at the UE,  $\mathbf{w}_i^{tx}$  is the TX beamforming vector at the BS cell,  $\mathbf{H}(t_i, f_k)$  is the narrowband channel response for the synchronization signal, and  $n_{ik}(t)$  is AWGN. Note that, as described above, we assume that each sub-signal is transmitted in a sufficiently narrow band that we can assume flat fading across the transmission. We let  $N_0$  denote the noise power spectral density.

We assume a standard multi-path channel model [12] where the time-varying channel response is given by

$$\mathbf{H}(t, f) = \frac{1}{\sqrt{L}} \sum_{\ell=1}^L \sqrt{g_{\ell}(t)} e^{2\pi j(f_{d,\ell} t - \tau_{\ell} f)} \mathbf{u}_{\ell}^{rx} \mathbf{u}_{\ell}^{tx*}, \quad (1)$$

where  $L$  is the number of paths and, for each path  $\ell$ ,  $g_{\ell}(t)$  is the time-varying channel power,  $f_{d,\ell}$  is the path Doppler shift, and  $\mathbf{u}_{\ell}^{rx}$  and  $\mathbf{u}_{\ell}^{tx}$  are the RX and TX spatial signatures of the path that depend on the angles of arrival and departure of the path from the antenna arrays.

In this work, we are interested in tracking the SNR in a single TX and RX pointing direction. As described in the previous subsection, the BS cell will use a fixed transmit direction and the UE receiver will scan  $N_{\text{dir}}$  beamforming directions and estimate the SNR separately in each direction. For the remainder of this paper, we focus on a subset of the transmission times  $i$  where the TX and the RX are pointed in a particular direction  $\mathbf{w}_i^{tx} = \mathbf{w}^{tx}$  and  $\mathbf{w}_i^{rx} = \mathbf{w}^{rx}$ , for some fixed  $\mathbf{w}^{tx}$  and  $\mathbf{w}^{rx}$ .

Given TX and RX directions  $\mathbf{w}^{tx}$  and  $\mathbf{w}^{rx}$ , define the wideband average channel gain as

$$G(t) = \frac{1}{W_{\text{tot}}} \int_{f_c - W_{\text{tot}}/2}^{f_c + W_{\text{tot}}/2} |\mathbf{w}^{rx*} \mathbf{H}(t, f) \mathbf{w}^{tx}|^2 df,$$

where the integral is over the total system bandwidth of  $W_{\text{tot}}$  at center frequency  $f_c$ . If the base station transmits at a power  $P_{tx}$ , then the average wideband SNR would be

$$\gamma(t) := \frac{G(t)P_{tx}}{N_0 W_{\text{tot}}}, \quad (2)$$

where  $W_{\text{tot}}$  is the total system bandwidth. We call  $\gamma(t)$  the *true wideband SNR*.

| Symbol           | Description   |
|------------------|---|
| $\gamma_i$       | Wideband true SNR   |
| $\hat{\gamma}_i$ | Raw SNR estimate of $\gamma_i$ from the synchronization signals |
| $\bar{\gamma}_i$ | Time-filtered SNR estimate of $\gamma_i$ from $\hat{\gamma}_i$  |

Table I: Symbols for the SNR and its estimates.

As stated before, since mmWave cells will not transmit a CRS, we wish to estimate the wideband SNR  $\gamma(t)$  from the synchronization signal. The wideband SNR can be estimated as follows: let  $E_s = \int |p_{ik}(t)|^2 dt$  denote the transmitted signal energy per sub-signal. We assume this does not vary with  $i$  or  $k$ . If the transmit power is  $P_{tx}$ , the signal duration is  $T_{\text{sig}}$  and there are  $N_{\text{sig}}$  signals,

$$E_s = \frac{P_{tx} T_{\text{sig}}}{N_{\text{sig}}}. \quad (3)$$

Now suppose that the receiver applies a matched filter for each sub-signal to obtain the statistic

$$z_{ik} = \frac{1}{\sqrt{E_s}} \int p_{ik}^*(t) r_{ik}(t) dt \quad (4)$$

$$= \sqrt{E_s} \mathbf{w}^{rx*} \mathbf{H}(t_i, f_k) \mathbf{w}^{tx} + v_{ik}, \quad v_{ik} \sim \mathcal{CN}(0, N_0).$$

It is easy to verify that if the frequency  $f_k$  is uniformly randomly distributed over the system bandwidth, then

$$\mathbb{E}[|z_{ik}|^2] = \frac{G(t) P_{tx}}{N_{\text{sig}}} + N_0.$$

Hence, we can form an unbiased estimate of  $\gamma(t)$  in (2) by

$$\hat{\gamma}_i = \frac{1}{N_0 T_{\text{sig}} W_{\text{tot}}} \sum_{k=1}^{N_{\text{sig}}} [|z_{ik}|^2 - N_0], \quad (5)$$

which sums the received power on the  $N_{\text{sig}}$  sub-signals and subtracts the noise.

#### D. Filtering Algorithms

Since  $\hat{\gamma}_i$  in (5) is an estimate of the wideband SNR that has been obtained starting from the synchronization signals, it may deviate from the true SNR due to noise. We call the measurement  $\hat{\gamma}_i$  the *raw* SNR. To reduce the noise, we can filter the raw SNR producing a time-averaged value that we will denote by  $\bar{\gamma}_i$ . We consider three possible filtering schemes [20]:

- *No filtering*: In this case, we simply take  $\bar{\gamma}_i = \hat{\gamma}_i$ .
- *First-order filtering*: This uses a simple low-pass filter:

$$\bar{\gamma}_i = (1 - \alpha) \bar{\gamma}_{i-1} + \alpha \hat{\gamma}_i, \quad (6)$$

for some constant  $\alpha \in (0, 1)$ .

- *Moving average filtering*: In this algorithm, we simply average the last  $M$  values,

$$\bar{\gamma}_i = \frac{1}{M} \sum_{j=1}^M \hat{\gamma}_{i-j+1}. \quad (7)$$

Therefore  $\bar{\gamma}_i$  is a *filtered SNR estimate* of  $\gamma_i$ , obtained starting from the noisy raw SNR  $\hat{\gamma}_i$ . Our goal is to find the optimum scheme to minimize the *average estimation error*  $e_i = \mathbb{E}[|\bar{\gamma}_i - \gamma_i|]$ , in order to derive an SNR stream that can be used to reliably estimate the channel quality.

### III. EXPERIMENTAL EVALUATION

#### A. Channel Modeling Overview

While there has been considerable progress in understanding the mmWave channel for long-range outdoor cellular links, most of the studies have been performed in stationary locations with minimal local blockage. For example, in the New York City studies in [12]–[15], the RX was placed in a fixed location on a cart. In addition, there were no obstacles in the immediate vicinity of the RX, such as a hand or a person, whose movement would cause signal variations due to blockage.

Unfortunately, measuring a wideband spatial channel model with dynamics is not possible with our current experimental equipment. Such a measurement would require that the TX and RX directions be swept rapidly during the local blockage event. Since our platform relies on horn antennas mounted on mechanically rotating gimbals, such rapid sweeping is not possible.

In this work, we thus propose the following alternate approximate method to generate realistic dynamic models for link evaluation:

- 1) We first randomly generate the number of paths, relative power, delay and angles of arrival and departure based on the wideband channel models in [12] and [15]. These models are based on extensive measurements in New York City in links similar to a likely urban micro-cellular deployment, and would reflect the characteristics of a stationary ground-level mobile with no motion nor local obstacles.
- 2) Combining the angles of arrivals and departure with the antenna array patterns at the BS and UE, we can then determine the spatial signatures  $\mathbf{u}_\ell^{rx}$  and  $\mathbf{u}_\ell^{tx}$  in (1). The randomly generated parameters from Step 1 will also provide the delay and power of each path, that we will denote by  $\tau_\ell$  and  $P_\ell$ , respectively.
- 3) We assume a random direction of motion of the UE receiver. Based on the UE velocity and angle of motion relative to the angle of arrivals of the path, we can compute the Doppler shifts  $f_{d,\ell}$  in (1) by  $f_{d,\ell} = f_{d,max} \cos \theta_\ell$ , where  $f_{d,max}$  is the maximum Doppler shift and  $\theta_\ell$  is the angle between the path angle of arrival and direction of motion.
- 4) Finally, if there were no local blockage, then the path powers  $g_\ell(t)$  in (1) could be fixed as  $g_\ell(t) = P_\ell$ , where the values  $P_\ell$  are the path powers generated in the static model in Step 1. To simulate local blockage, we assume that these powers will be modulated as

$$g_\ell(t) = \beta P_\ell h(t), \quad (8)$$

where  $h(t)$  is a time-varying scaling factor accounting for the blockage and  $\beta$  is a scaling factor. Since there

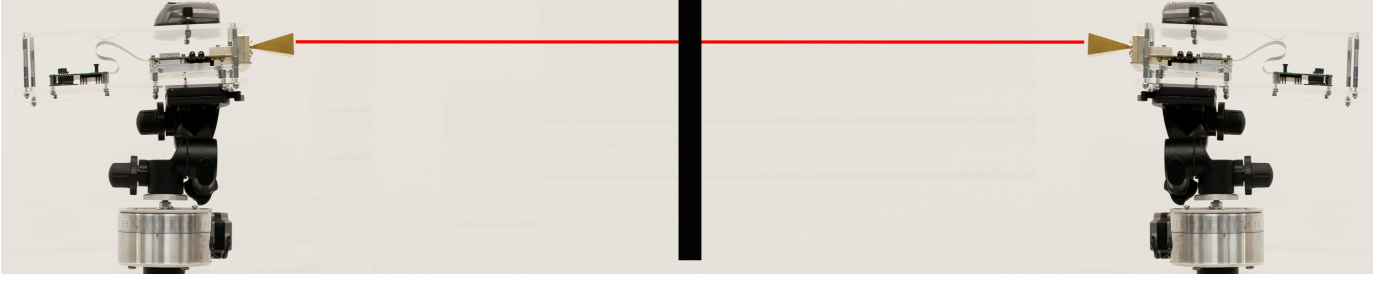


Figure 2: Our mmWave testbed. We introduce an obstacle (person walking, hand, metal plate) in front of the receiver to observe the received power drop.

are no statistical models for the blockage dynamics, we measure traces of  $h(t)$  experimentally in various blockage scenarios. The factor  $\beta$  can then be adjusted to set a desired test SNR, according to the envisioned target rate a mmWave user is expected to reach. We refer to Section IV for further details on the choice of this parameter.

This four step procedure thus provides a semi-statistical model, in which (i) the spatial characteristics of the channel are determined from static statistical models derived from outdoor measurements and (ii) local blockage events are measured experimentally and modulated on top of the static parameters.

An important simplification in (8) is that we assume that the local blockage  $h(t)$  equally attenuates all paths, which may not be realistic. For example, a hand may block only paths in a limited range of directions. However, this work considers the SNR tracking in only one direction at a time. In any fixed direction, most of the power is contributed only from paths within a relatively narrow beamwidth and thus the approximation that the paths are attenuated together may be reasonable.

### B. Channel Sounding System

We will call the scaling term  $h(t)$  in (8) the *local blockage factor*<sup>1</sup>. The key challenge in measuring the dynamics of local blockage is that we need relatively fast measurements. To perform these fast measurements, we used the experimental channel sounding system in Figure 2: a high-bandwidth baseband processor, built on a PXI (a rugged PC-based platform for measurement and automation systems) from National Instruments, which engineers a real-world mmWave link. The transmitter and receiver operate in two separate boxes, each of which have the parts listed below:

- (i) an 8-slot chassis, capable of holding a variety of expansion cards.
- (ii) a 1.73 GHz quad-core PXIe controller that runs a realtime operating system (RTOS) called PharLap, and communicates with the computer used to run the experiments through an Ethernet connection to coordinate the operation of each peripheral card in the chassis.
- (iii) two FPGA cards for the baseband signal processing.

<sup>1</sup>Note that the absolute value of  $h(t)$  is immaterial, since the total channel power will be scaled by the factor  $\beta$  in (8) to target a particular SNR.

- (iv) a FlexRIO adapter module (FAM) card and a converter between the baseband signal and an IF signal, which are connected to the antenna.
- (v) mmW Converters, to convert the IF signal to mmWave in the range of 57–63 GHz. The IF signal is mixed with the output of a local oscillator (LO), filtered, amplified, and sent over a waveguide output. We use 23 dBi directional horn antennas (manufactured by Sage millimeter) to interface with the waveguide. This converter works in tandem with a power supply and a controller card. An identical converter at the receiver performs the down-conversion from mmWave frequencies to IF.

To sound the channel, we used a standard frequency-domain method: the *transmitter* sent a continuous repeating pattern created from an IFFT of a 128 point pseudo random QPSK sequence. We will call each group of 128 samples a symbol. The sample rate is 130 MHz corresponding to a symbol period of approximately 1  $\mu$ s. Note that this symbol period is larger than the maximum delay spread. The *receiver* segments the received time domain sequence into symbols, takes the FFT of each symbol and derotates it by the frequency-domain representation of the transmitted sequence. Since the transmitted signal is periodic, the derotated signal at the receiver will provide an estimate of the frequency-domain response of the channel. To reduce the effect of the noise, the sequence is averaged over 32 symbols, providing one averaged response every  $32 \times 1 = 32$   $\mu$ s. The averaged response is then converted to time-domain, to produce the power delay profile (PDP) of the channel.

The phase noise at the receiver can be large (the manufacturer specification is up to  $-80$  dBc). This is a common problem in many mmWave RF units. A characterization of this receiver in [21] found the maximum frequency deviation to be up 50 kHz, which would be too large to leave uncompensated. To compensate for the phase noise, in each 32 symbol measurement period the receiver derotated the signal by 9 frequency hypotheses spaced uniformly from  $-50$  to  $50$  kHz, and a potential PDP was generated from each of the 9 different hypotheses. The PDP with the maximum peak was then selected amongst the 9 hypotheses. After this phase compensation, the received symbols are sufficiently coherent over the 32  $\mu$ s period needed for a new averaged response to be provided.

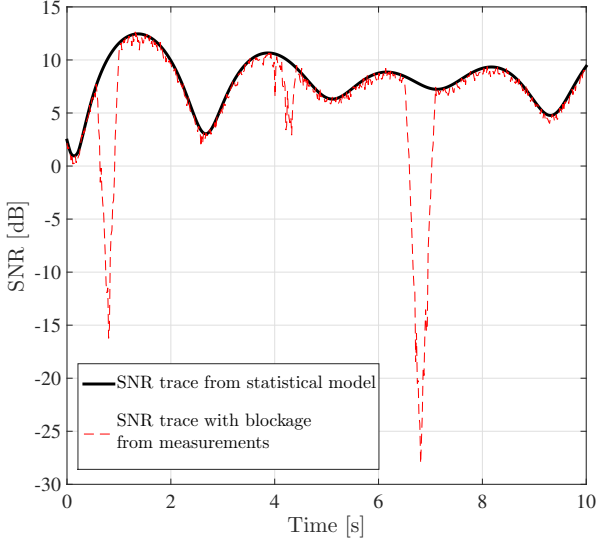


Figure 3: SNR trace perceived when receiving the synchronization signals. The solid line is obtained by simulating the statistical channel described in [12] and [15] (without local obstacles). In the dashed line, the experimentally measured local blockage dynamics are modulated on top of the statistical trace. The blockage is referred to a person walking multiple times between the transmitter and the receiver.

### C. Measurement of Local Blockage

Using the above system, the blockage experiments were conducted by placing the transmitter and the receiver on a one-meter high pedestal, facing each other, at a distance of 4 meters. A laser pointer was used to improve the alignment between the two devices.

After this set-up, the system is then run to continuously collect PDPs during a blockage event. Blockage events are simulated by placing moving obstacles between the transmitter and the receiver. In this work, we considered three common blockage events: (i) a person walking (or running) between TX and RX; (ii) a wood (or metal) plate held between the two communication edges; (iii) a hand holding a cellular phone.

The system was run during each of these blockage events for a total time of 10 seconds. During this time, PDPs were measured at a rate of one PDP per 32  $\mu$ s. We found that the dynamics of the channel varied considerably slower than this rate, so we decimated the results by a factor of four, recording one PDP per 128  $\mu$ s. Since each experiment was run for 10 seconds, each experiment resulted in  $10^7/128 = 78125$  PDP recordings.

To determine the local blockage function, we are only interested in the line-of-sight path. The power on this path was determined from the maximum peak in the PDP. Reflected paths would appear in other samples and thus be rejected. This received power then provides the trace for the local blockage function  $h(t)$  in (8). As described above, this local blockage function is then used to modulate the time-varying channel response obtained from the statistical channel model.

As an example, Figure 3 shows an SNR trace in which the

| Description   | 50 <sup>th</sup> percentile    | 5 <sup>th</sup> percentile      |
|---|--------------------------------|---------------------------------|
| LTE spectral efficiency<br>$\rho$ (bit/s/Hz/ $W_{\text{tot}}$ ) (from [22]) | <b>3.28</b>                    | <b>0.154</b>                    |
| LTE rate (Mbps)<br>( $R_\mu = \rho \cdot W_{\text{tot}}$ )                  | $3.28 \cdot 50 = \mathbf{164}$ | $0.154 \cdot 50 = \mathbf{7.7}$ |
| mmWave rate (Mbps)<br>(from [23], $R_{\text{mmW}} \simeq 9R_\mu$ )          | <b>1480</b>                    | <b>70</b>                       |

Table II: Cell user 4G-LTE and expected 5G rate, for average-cell-position users (50<sup>th</sup> percentile) and cell-edge users (5<sup>th</sup> percentile). For the LTE case, we refer to a DL SU-MIMO  $4 \times 4$  TDD baseline for a microwave system using 50 MHz of bandwidth. For the mmWave case, we refer to a system with 500 MHz of bandwidth and a single user.

blockage event is referred to a person walking multiple times between the transmitter and the receiver.

### D. Evaluation Results

Once the SNR trace  $\gamma(t)$  from the synchronization signals has been obtained, combining the simulated statistical channel described in [12] and [15] with the local blockage dynamics measured experimentally, the raw SNR  $\hat{\gamma}(t)$  can be estimated from the synchronization signals following Section II-C. In Section IV we describe the system parameters that we use in our simulations, while in Section V we analyze and compare the performance of the presented linear filters, applied to the raw SNR trace, to obtain the estimate  $\bar{\gamma}(t)$ .

## IV. SIMULATION PARAMETERS

In this section, we derive some parameters that we will use in the SNR tracking simulations: (i) the scaling factor  $\beta$  of Equation (8), to set a desired test SNR, and (ii) the SNR trace downsampling factor.

### A. SNR scaling factor $\beta$

As previously asserted, the scaling factor  $\beta$  in (8) is selected to bring the average SNR to some desired test level. We consider two test cases:

- 1) the user belongs to the 50<sup>th</sup> percentile, so it presents average propagation conditions;
- 2) the user belongs to the 5<sup>th</sup> percentile, to simulate the 5% worst user rate at cell edges.

For each case, the target test SNR is obtained by: (i) determining a reliable 4G-LTE target rate for the user, according to [22]; (ii) determining the corresponding mmWave target rate, according to [23]; and (iii) finding the corresponding target test SNR through a Shannon capacity evaluation.

In order to find a reliable data rate for the two user cases we are considering, we refer to the actual LTE 3GPP user data rate. We consider the performance of the DL SU-MIMO  $4 \times 4$  TDD baseline in [22], for a microwave system using 50 MHz of bandwidth. In Table II, we show the cell user spectral efficiency  $\rho$  that we use to compute the LTE data rate  $R_\rho$  (actually  $R_\rho = \rho \cdot W_{\text{tot}}$ ).

The corresponding DL data rate for a mmWave system with 500 MHz of bandwidth can be determined referring to



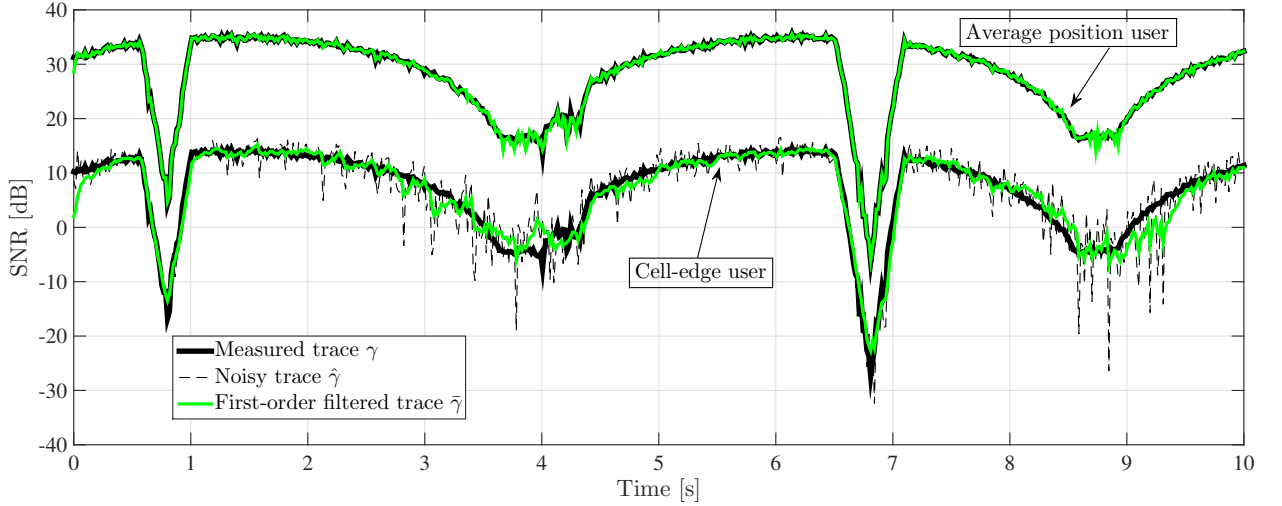


Figure 4: SNR trace  $\gamma(t)$  together with its raw version  $\hat{\gamma}(t)$  and its estimation  $\tilde{\gamma}(t)$  after different filtering schemes are applied. The upper lines refer to the SNR of a 50<sup>th</sup> percentile typical user, while the lower lines refer to the SNR of a 5<sup>th</sup> percentile edge user.

[23], where it is reported that the data rate of a mmWave user is expected to be around 9 times higher than the rate of current LTE systems. According to this result, Table II reports the corresponding rates that can realistically be achieved by mmWave users.

Based on the mmWave user data rate, we can estimate the corresponding target SNR  $\gamma_t$  using the Shannon capacity:

$$R = \delta \cdot W_{\text{tot}} \cdot \log_2(1 + \gamma_t) \implies \gamma_t = 2^{\frac{R}{\delta \cdot W_{\text{tot}}}} - 1 \quad (9)$$

where  $R$  is the data rate,  $W_{\text{tot}}$  is the system bandwidth (500 MHz for the mmWave system we are considering), and  $\gamma_t$  is the target data SNR.  $\delta = 0.8$  is a parameter that accounts for a 20% control overhead [12]. Solving (9), we obtain the target SNR  $\gamma_t$ .

The value  $\gamma_t$  is the wideband SNR we would expect on a data channel. The data channel would be received with the BS and UE performing beamforming. However, the synchronization signals would be transmitted omni-directionally and thus would be received at a lower SNR. In the experiments below, following [12], we will assume that the BS cell has  $N_{tx} = 64$  antennas, allowing up to a 18 dB beamforming gain. This gain would not be available for the synchronization and thus the synchronization signals would be received at a much lower SNR – this is one of the main challenges in SNR tracking. Thus, we assume that the wideband SNR (in linear scale) should be  $\gamma_t/N_{tx}$ .

To set this SNR, we first generate a random trace of using the statistical model. Then, we set the factor  $\beta$  in (8) to scale the average value of the wideband SNR  $\gamma(t)$  in the experiment to the desired target level  $\gamma_t/N_{tx}$ . This generates the sequence for the wideband SNR  $\gamma(t)$ . The raw estimate of the SNR  $\hat{\gamma}(t)$  is then computed according to Section II.

### B. SNR Trace Downsampling Factor

As we stated in Section III-C, the measured SNR trace is composed of 78125 samples, one every 128  $\mu s$ . According to Section II and the results in [24], we assume that each synchronization signal is transmitted periodically once every  $T_{\text{per}} = 1$  ms for a duration of  $T_{\text{sig}} = 10 \mu s$ , to maintain an overhead of 1%. Moreover, we also assume that the user directionally receives such signals by performing an exhaustive search of the angular space through  $N_{\text{slot}} = 16$  directions. Therefore, the transmitter and the receiver will be perfectly aligned just once every  $N_{\text{slot}}T_{\text{per}} = 16$  ms. For this reason, the original SNR trace has been downsampled, keeping just one sample every 16 ms.

## V. PERFORMANCE EVALUATION

In Section V-A, we analyze and compare the performance of the filtering algorithms described in Section II-D. The goal is to determine the filter that minimizes the estimation error  $e(t) = \mathbb{E}[|\tilde{\gamma}(t) - \gamma(t)|]$ , for different user propagation characteristics (50<sup>th</sup> and 5<sup>th</sup> percentiles). Furthermore, Section V-B shows how the estimation error changes when considering different SNR regimes.

### A. Filters performance comparison

In Figure 4, we plot the SNR trace  $\gamma(t)$ , whose blockage events refer to a person walking multiple times between the transmitter and the receiver. The upper line refers to a 50<sup>th</sup> percentile typical user and the lower line to a 5<sup>th</sup> percentile edge user. The figure also shows the noisy version  $\hat{\gamma}(t)$  of the SNR trace, together with its estimate  $\tilde{\gamma}(t)$  after the presented linear filters have been applied. Two different scaling factors  $\beta$  have been applied, when computing the SNR trace from the synchronization signals, according to the two user propagation regimes.

We see that, for low SNR regimes, the raw SNR trace  $\hat{\gamma}(t)$  shows a very noisy trend, which is considerably different from

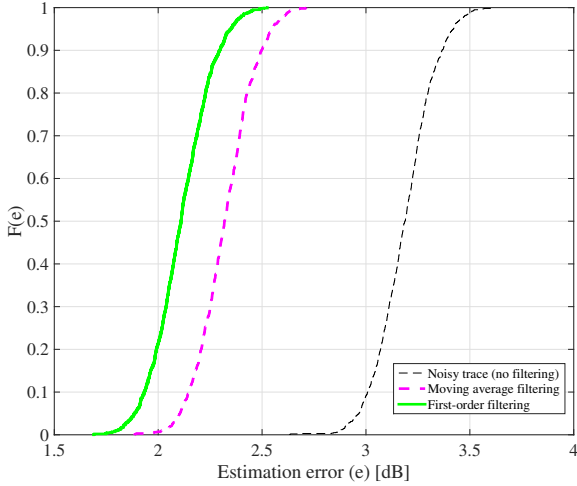


Figure 5: CDF of the estimation error  $e(t) = |\hat{\gamma}(t) - \gamma(t)|$  for a 5<sup>th</sup> percentile edge user, when different linear filters are applied to the noisy SNR trace  $\hat{\gamma}(t)$ .

its original version. The reason is that, when the user receives the synchronization signals with very low power (e.g., when located at the cell edge), the noise component dominates the SNR unbiased estimate in (5), and therefore the raw SNR substantially differs from  $\gamma(t)$ . A filtering algorithm is thus required, to recover a stream  $\hat{\gamma}(t)$  that can be used to more accurately estimate the channel. The main concern is that it is hard to discern between the downspikes which refer to an actual blockage and those which accidentally manifested due to the additive noise. In such a way, the detection of real radio link failure situations might be distorted and might lead to false alarm or missed blockage detection events.

However, a simple first-order filter can produce an estimated SNR trace  $\hat{\gamma}(t)$  that appears very similar to the measured one. Therefore, even without designing much more complex and expensive nonlinear adaptive filters, we can properly restore the desired SNR stream and perform reliable link failure detection and channel estimation. It should finally be noted that this filter requires a transient phase before reaching its normal operation, as can be seen in the first milliseconds of the traces in Figure 4.

It is interesting to note that, when considering a good SNR regime (upper lines of Figure 4, simulating a 50<sup>th</sup> percentile user), even the raw SNR trace  $\hat{\gamma}(t)$  (when no filters are applied) almost overlaps with its measured original version. Therefore, when an average position mmWave user receives uncorrupted synchronization signals, it estimates an SNR trace  $\hat{\gamma}(t)$  that sufficiently resembles the measured one, and can hence perform an adequately reliable channel estimation without any further signal processing.

In Figure 5 we plot the CDFs of the estimation error for a 5<sup>th</sup> percentile edge user, when different linear filters are applied to the noisy SNR trace  $\hat{\gamma}(t)$ . The trace after a first-order filter is used shows much better performance with respect to the moving-average filtered trace which, besides

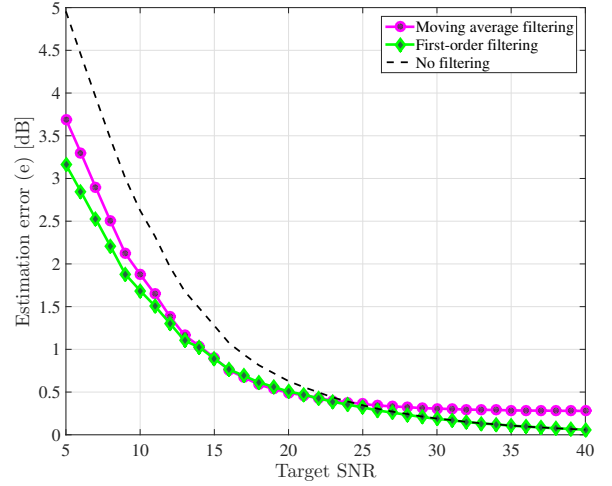


Figure 6: Average estimation error  $e(t) = \mathbb{E}[|\hat{\gamma}(t) - \gamma(t)|]$  vs. target SNR, for different linear filter configurations.

its poor efficiency, is also affected by a non-negligible delay. Therefore, among the options we considered, a first-order filter is the best choice to reduce the estimation error and properly track the SNR trace.

#### B. Analysis of the estimation error

In Figure 6, we show the average estimation error  $e(t) = \mathbb{E}[|\hat{\gamma}(t) - \gamma(t)|]$  versus different target SNR values  $\gamma_t$ , obtained by adjusting the scaling factor  $\beta$  in Equation (8). Multiple linear filter algorithms are applied to the raw SNR trace.

For low SNR regimes, we recognize again the better performance of the first-order filter, with respect to the capabilities of the moving-average filter. However, it is interesting to note that, after a certain threshold ( $\gamma_t \geq 24$  dB), the moving-average is an even worse estimate than the noisy SNR trace  $\hat{\gamma}(t)$  where no filters or further digital signal processing have been applied. Moreover, in the same high-SNR range, the trend of  $\hat{\gamma}(t)$  almost overlaps with the performance of the first-order filter in Figure 6. This agrees with the result of Subsection V-A where we stated that, when simulating a 50<sup>th</sup> percentile user, the AWGN noise does not significantly affect the estimated raw SNR trace  $\hat{\gamma}(t)$ , which therefore faithfully tracks the actual SNR evolution.

## VI. CONCLUSIONS AND FUTURE WORK

A key concern for the feasibility of mmWave system is the rapid channel dynamics. Two broad questions need understanding: how fast do channels actually change and how can systems be designed to deal with these variations. This paper has attempted to develop some fundamental understanding in the context of one particularly important problem – namely the tracking of SNR. We have considered a simplified procedure to estimate the SNR that can be readily implemented in next generation systems using synchronization signals. These signals will be necessary for initial access and thus will not

introduce further overhead. Simple estimates for the SNR for these were derived. The methods were then evaluated in a novel semi-statistical model, where the spatial characteristics were derived from an existing statistical model based on outdoor measurements and the local blockage was derived from new experimental measurements.

Our high level finding is that the SNR can be mostly tracked within a few dB of error, even when the measurements are in very low SNR. Nevertheless, using very simple filtering mechanisms, the SNR tracking does incur some delay, particularly during periods of very rapid changes.

Further work is still needed. Most directly, it is useful to test nonlinear and/or adaptive mechanisms that could track this SNR more effectively. Also, this SNR tracking can then be used to assess the effects on other higher layer functions including rate prediction, handover and radio link failure detection.

## REFERENCES

- [1] DMC R&D Center Samsung Electronics Co., "5G vision," Feb. 2015, White Paper. [Online]. Available at <http://www.samsung.com/global/business-images/insights/2015/Samsung-5G-Vision-0.pdf>.
- [2] A. Osseiran, F. Boccardi, V. Braun, K. Kusume, P. Marsch, M. Maternia, O. Queseth, M. Schellmann, H. Schotten, H. Taoka *et al.*, "Scenarios for 5G mobile and wireless communications: the vision of the METIS project," *IEEE Communications Magazine*, vol. 52, no. 5, pp. 26–35, 2014.
- [3] F. Khan and Z. Pi, "mmWave mobile broadband (MMB): Unleashing the 3–300 GHz spectrum," in *34th IEEE Sarnoff Symposium*, May 2011.
- [4] T. S. Rappaport, S. Sun, R. Mayzus, H. Zhao, Y. Azar, K. Wang, G. N. Wong, J. K. Schulz, M. Samimi, and F. Gutierrez, "Millimeter Wave Mobile Communications for 5G Cellular: It Will Work!" *IEEE Access*, vol. 1, pp. 335–349, May 2013.
- [5] S. Rangan, T. S. Rappaport, and E. Erkip, "Millimeter-wave cellular wireless networks: Potentials and challenges," *Proceedings of the IEEE*, vol. 102, no. 3, pp. 366–385, March 2014.
- [6] T. S. Rappaport, R. W. Heath Jr, R. C. Daniels, and J. N. Murdock, *Millimeter wave wireless communications*. Pearson Education, 2014.
- [7] J. Lu, D. Steinbach, P. Cabrol, and P. Pietraski, "Modeling the impact of human blockers in millimeter wave radio links," *ZTE Commun. Mag.*, vol. 10, no. 4, pp. 23–28, 2012.
- [8] S. Sesia, I. Toufik, and M. Baker, *LTE, The UMTS Long Term Evolution: From Theory to Practice*. Wiley Publishing, 2009.
- [9] S. Schwarz, C. Mehlführer, and M. Rupp, "Calculation of the spatial preprocessing and link adaption feedback for 3GPP UMTS/LTE," in *Proc. IEEE Conf. Wireless Advanced (WiAD)*. IEEE, 2010, pp. 1–6.
- [10] C. N. Barati, S. A. Hosseini, S. Rangan, P. Liu, T. Korakis, S. S. Panwar, and T. S. Rappaport, "Directional cell discovery in millimeter wave cellular networks," *IEEE Transactions on Wireless Communications*, vol. 14, no. 12, pp. 6664–6678, Dec 2015.
- [11] C. N. Barati, S. A. Hosseini, M. Mezzavilla, S. Rangan, T. Korakis, S. S. Panwar, and M. Zorzi, "Directional initial access for millimeter wave cellular systems," *arXiv preprint arXiv:1511.06483*, 2015.
- [12] M. R. Akdeniz, Y. Liu, M. K. Samimi, S. Sun, S. Rangan, T. S. Rappaport, and E. Erkip, "Millimeter wave channel modeling and cellular capacity evaluation," *IEEE Journal on Selected Areas in Communications*, vol. 32, no. 6, pp. 1164–1179, June 2014.
- [13] M. K. Samimi, T. S. Rappaport, and G. R. MacCartney, "Probabilistic omnidirectional path loss models for millimeter-wave outdoor communications," *IEEE Wireless Communications Letters*, vol. 4, no. 4, pp. 357–360, Aug 2015.
- [14] T. S. Rappaport, G. R. MacCartney, M. K. Samimi, and S. Sun, "Wide-band millimeter-wave propagation measurements and channel models for future wireless communication system design," *IEEE Transactions on Communications*, vol. 63, no. 9, pp. 3029–3056, Sept 2015.
- [15] M. K. Samimi and T. S. Rappaport, "3-D statistical channel model for millimeter-wave outdoor mobile broadband communications," in *Proc. ICC*, June 2015, pp. 2430–2436.
- [16] P. A. Eliahi and S. Rangan, "Stochastic dynamic channel models for millimeter cellular systems," in *Proc. IEEE Computational Advances in Multi-Sensor Adaptive Processing (CAMSAP)*. IEEE, 2015, pp. 209–212.
- [17] S. Ferrante, T. Deng, R. Pragada, and D. Cohen, "mm Wave initial cell search analysis under UE rotational motion," in *Proc. IEEE Ubiquitous Wireless Broadband (ICUWB)*. IEEE, 2015, pp. 1–7.
- [18] S. Sun, T. S. Rappaport, R. W. Heath, A. Nix, and S. Rangan, "MIMO for millimeter-wave wireless communications: beamforming, spatial multiplexing, or both?" *IEEE Communications Magazine*, vol. 52, no. 12, pp. 110–121, December 2014.
- [19] R. W. Heath Jr, N. Gonzalez-Prelcic, S. Rangan, W. Roh, and A. Sayeed, "An overview of signal processing techniques for millimeter wave MIMO systems," *arXiv preprint arXiv:1512.03007*, 2015.
- [20] J. Proakis and M. Salehi, *Digital Communications*, ser. McGraw-Hill International Edition. McGraw-Hill, 2008.
- [21] A. Dhananjay, "Iris: Mitigating phase noise in millimeter wave OFDM systems," Ph.D. dissertation, New York University (NYU), 2015.
- [22] 3GPP, Further advancements for E-UTRA physical layer aspects, TR 36.814 (release 9), 2010.
- [23] F. Boccardi, R. W. Heath, A. Lozano, T. L. Marzetta, and P. Popovski, "Five disruptive technology directions for 5G," *IEEE Communications Magazine*, vol. 52, no. 2, pp. 74–80, February 2014.
- [24] M. Giordani, M. Mezzavilla, C. N. Barati Nt., S. Rangan, and M. Zorzi, "Comparative analysis of initial access techniques in 5G mmwave cellular networks," in *Annual Conference on Information Science and Systems (CISS)*, Princeton, USA, 2016.